Langmuir

Article

pubs.acs.org/Langmuir

Size-Dependent MRI Relaxivity and Dual Imaging with $Eu_{0.2}Gd_{0.8}PO_4{\cdot}H_2O$ Nanoparticles

Yichen Li, Tao Chen, Weihong Tan, and Daniel R. Talham*

Department of Chemistry, University of Florida, Gainesville, Florida 32611-7200, United States

Supporting Information

ABSTRACT: Three different sizes of $Eu_{0.2}Gd_{0.8}PO_4{\cdot}H_2O$ nanoparticles have been prepared to investigate the particle size influence on water proton relaxivity. Longitudinal relaxivity (r_1) values increase for smaller particles, reaching as high as r_1 = 6.13 mM^{-1} s^{-1} for a sample of 40 ± 4 nm particles, which, with a ratio of transverse/longitudinal relaxivity, r_2/r_1 = 1.27, are shown to be effective positive contrast agents. The correlation between relaxivity and the surface-to-volume ratio implies that access to surface Gd^{3+} sites is the principal factor affecting relaxivity. On the other hand, although ionic molar relaxivity decreases for larger particles, the relaxivity per particle can be significantly greater. Gadolinium-based nanoparticles doped with fluorescent lanthanide elements have attracted attention for their dual-imaging abilities, combining magnetic resonance imaging (MRI) and fluorescence imaging agents. In both *in vitro* experiments with HeLa cells and *in vivo* experiments with *C. elegans*, strong red fluorescence is observed from $Eu_{0.2}Gd_{0.8}PO_4{\cdot}H_2O$ with high resolution, demonstrating the parallel use of the particles as fluorescence imaging agents.

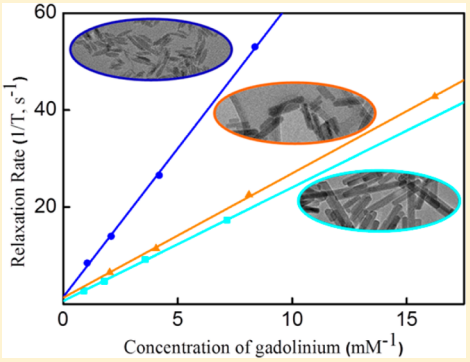

1. INTRODUCTION

Multifunctional nanoparticles elicit considerable attention due to their ability to serve simultaneously as agents for important tasks such as MRI, fluorescence imaging, controlled drug release, and specific targeting.[1−3] A variety of material platforms have been used to develop multiple functions, including gold, silica, polymer, and magnetic oxide nanoparticles.[4−7] Gadolinium ion-based nanoparticles such as Gd_2O_3, $KGdF_4$, and $GdPO_4$ are a promising category due to their intrinsic ability to affect water proton relaxation and serve as potential T_1 or T_2 contrast agents.[8−10]

Combining fluorescent bioimaging with MRI capabilities is attractive because the greater sensitivity and resolution of fluorescence imaging can be used to complement MRI capabilities.[3,8,9,11] Several nanoparticle-based systems have been developed for this purpose, such as superparamagnetic Fe_3O_4 nanoparticles conjugated with fluorescent quantum dots and organic fluorophores immobilized on Gd_2O_3 nanoparticles.[8,12] The mixing of different lanthanide ions in a single-phase system provides an effective way to achieve particles that combine fluorescence imaging and MRI easily while avoiding potential complication associated with more complex architectures.[13−17] Circumventing the need for quantum dots or organic fluorophores, lanthanide ions such as Eu^{3+} and Tb^{3+} show extraordinary fluorescent properties, including large Stokes shifts, long lifetimes, and narrow emission lines.[13,17,18] With seven unpaired electrons, Gd^{3+} forms the basis of the most widely used T_1 contrast agents.[19] As a result of these advantages, gadolinium-based nanoparticles have become a suitable platform for doping with luminescent lanthanide ions to achieve dual-mode imaging agents. Previously, Shi et al.[16] used Eu^{3+}-doped Gd_2O_3 hybrid nanoparticles to label human mesenchymal stem cells (hMSCs), which was confirmed by confocal laser scanning microscopy. In addition, europium-doped gadolinium sulfide ($GdS:Eu^{3+}$) was successfully applied as a fluorescent imaging agent for breast cancer cells (SK-BR-3).[15] In a third example, Ren et al.[13] used Eu^{3+}-doped $GdPO_4$ nanorods to observe red luminescence from labeled HeLa cells.

Following our earlier report[10] exploring MRI contrast generation with gadolinium phosphate particles stabilized with phosphate-terminated oligonucleotides, we became interested in the $Eu_xGd_{1-x}PO_4{\cdot}H_2O$ system. The present report describes the synthesis of $Eu_{0.2}Gd_{0.8}PO_4{\cdot}H_2O$, and we show that suspensions can be stabilized by the phosphate-containing modifier, *N*-phosphonomethyl iminodiacetic acid (PMIDA). The PMIDA-modified particles are shown to be compatible with HeLa and A549 cells in viability studies and can be used to generate fluorescent images of the cells. The particles also enhance water proton relaxivity and are demonstrated to be MRI contrast agents. Our study contributes to a range of relaxivity values reported for the $GdPO_4{\cdot}H_2O$ and $Eu_xGd_{1-x}PO_4{\cdot}H_2O$ systems.[10,13,20,21] Differing particle size is likely one of the parameters contributing to the range of reported values,[19,22−26] so to understand the particle size dependence better, three different samples, ranging from ∼40 to ∼140 nm, are investigated.

Received: February 14, 2014
Revised: April 25, 2014
Published: May 13, 2014

   dx.doi.org/10.1021/la500602x | *Langmuir* 2014, 30, 5873−5879

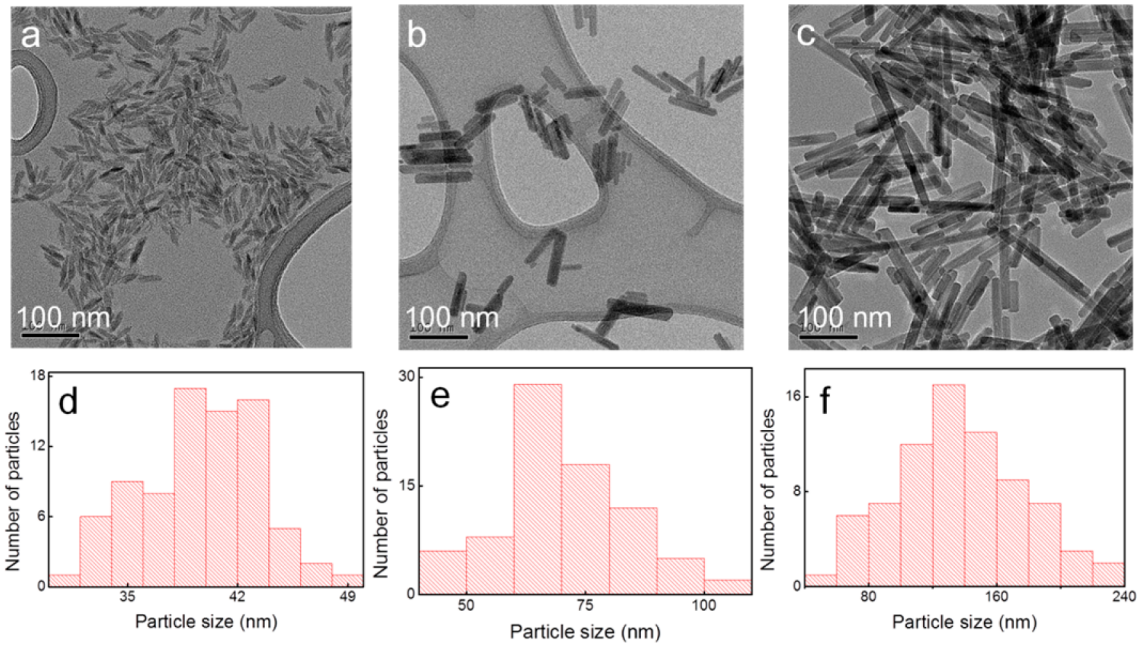

Figure 1. TEM images of PMIDA-modified $Eu_{0.2}Gd_{0.8}PO_4{\cdot}H_2O$, samples **1** (a), **2** (b), and **3** (c); particle length distributions obtained from the TEM images (d) sample **1**: 40 ± 4 nm; (e) sample **2**: 71 ± 14 nm; and (f) sample **3**: 145 ± 36 nm.

2. MATERIALS AND METHODS

2.1. Synthesis of $Eu_{0.2}Gd_{0.8}PO_4{\cdot}H_2O$ Nanoparticles. *2.1.1. Sample 1.* The synthesis of nanoparticles is based on procedures developed in our previous report with a few modifications.[10] The nanoparticles are obtained by combining two precursor surfactant mixtures, one containing the metal ions and the other the phosphate ions. The metal ions, 400 mg of $Gd(NO_3)_3{\cdot}6H_2O$ and 100 mg of $Eu(NO_3)_3{\cdot}6H_2O$, in 5 mL of water are added to a solution of IGEPAL CO-520 (20 mL) dissolved in 100 mL of cyclohexane under vigorous stirring. In a separate suspension, $NaH_2PO_4{\cdot}H_2O$ (700 mg) in 5 mL of water is combined with a solution of IGEPAL CO-520 (20 mL) dissolved in 100 mL of cyclohexane. The two suspensions were stirred separately for 1 h at room temperature, following which they were combined by the dropwise addition of the phosphate suspension to the metal ion suspension within a time period of 30 min. Once the addition was complete, the mixture was stirred vigorously for 3 h before the microemulsion was broken with 200 mL of acetone. The nanoparticles were collected by centrifugation and washed with water and acetone. The surface modification of the nanoparticles was performed by dispersing 20 mg of the nanoparticles in 1 mL of water followed by the addition of 30 mg of $Gd(NO_3)_3{\cdot}6H_2O$ and sonicating for 20 min. To this suspension, 3 mL (pH 7) of 60 mg of PMIDA was added. The mixture was left to sonicate for another 1 h, after which the nanoparticles were collected by centrifugation, washed with water, and redispersed in water for later use. Sample **1**: 40 ± 4 nm, white color; ICP (Gd/Eu in mg/L) 32.54/7.58; XRD, all of the peaks can be indexed to the hexagonal phase of $GdPO_4{\cdot}H_2O$ (JCPDS no. 39-232) or $EuPO_4{\cdot}H_2O$ (JCPDS no. 20-1044); IR, <1250 cm^{-1} characteristic of $(PO_4)^{3-}$ vibrations, 2920 and 2851 cm^{-1} associated with the asymmetric (ν_{as}) and symmetric (ν_s) stretching vibrations of methylene ($-CH_2$) groups of PMIDA.

2.1.2. Sample 2. Hydrothermal methods were used, combining a mixture of Eu^{3+} and Gd^{3+} ions with $(NH_4)_2HPO_4$.[27] A solution of 400 mg of $Gd(NO_3)_3{\cdot}6H_2O$ and 100 mg of $Eu(NO_3)_3{\cdot}6H_2O$ in 15 mL of water was combined with a solution of 0.5734 g of $(NH_4)_2HPO_4$ in 15 mL of water and stirred for 20 min before transferring the entire contents into a 130 mL Teflon-lined autoclave. The autoclave was sealed and maintained at 130 °C for 14 h. After cooling to room temperature, the precipitate was separated by centrifugation and washed with water. The same surface modification described for sample **1** was used. Sample **2**: 71 ± 14 nm, white color; ICP (Gd/Eu in mg/L) 41.20/10.05; XRD, all of the peaks can be indexed to the hexagonal phase of $GdPO_4{\cdot}H_2O$ (JCPDS no. 39-232) or $EuPO_4{\cdot}H_2O$ (JCPDS no. 20-1044); IR, <1250 cm^{-1} characteristic of $(PO_4)^{3-}$ vibrations, 2920 and 2851 cm^{-1} associated with the asymmetric (ν_{as}) and symmetric (ν_s) stretching vibrations of methylene ($-CH_2$) groups of PMIDA.

2.1.3. Sample 3. The same process described for sample **2** was used, changing the precursor solutions to 400 mg of $Gd(NO_3)_3{\cdot}6H_2O$ plus 100 mg of $Eu(NO_3)_3{\cdot}6H_2O$ in 10 mL of water and 700 mg of $NaH_2PO_4{\cdot}H_2O$ in 10 mL of water. The same surface modification was used. Sample **3**: 145 ± 36 nm, white color; ICP (Gd/Eu in mg/L) 45.34/11.41; XRD, all of the peaks can be indexed to the hexagonal phase of $GdPO_4{\cdot}H_2O$ (JCPDS no. 39-232) or $EuPO_4{\cdot}H_2O$ (JCPDS no. 20-1044); IR, <1250 cm^{-1} characteristic of $(PO_4)^{3-}$ vibrations, 2920 and 2851 cm^{-1} associated with the asymmetric (ν_{as}) and symmetric (ν_s) stretching vibrations of methylene ($-CH_2$) groups of PMIDA.

2.2. Characterization. Particle size analysis was conducted using a JEOL-2010F high-resolution transmission electron microscope (TEM) at 200 kV. The TEM grids (an ultrathin carbon film on a holey carbon support film, 400 mesh, copper) were prepared by dropping 40 μL of a solution containing 5 mg of sample dispersed in 1 mL of water. Powder X-ray diffraction (XRD) was recorded on a Philips X'Pert MRD materials research diffractometer using a Cu Kα source. For the XRD measurements, particles (10 mg) were mounted with double-sided tape on a glass slide, and the range was set from 10 to 80° with a step size of 0.008°. The metal composition and the Gd ion concentration of the samples for relaxivity measurements were determined with an inductively coupled plasma atomic emission spectrometer (ICP-AES, PerkinElmer Optima 3200 RL) and an energy-dispersive X-ray spectrometer (EDS, Oxford Instruments EDS X-ray microanalysis system coupled to the HRTEM microscope). FT-IR spectra were recorded on a Nicolet 6700 Thermo Scientific spectrophotometer. Fluorescence spectra were collected by a Photon Technology International (PTI) photon-counting fluorescence spectrophotometer.

2.3. Relaxivty Measurements and Magnetic Resonance Imaging. All MR relaxation time measurements were carried out at 1.4 T on a Minispec mq60 TD-NMR contrast agent analyzer (Bruker Optics, Billerica, MA, USA) at a constant temperature of 37 °C. T_1 relaxation times were measured using an inversion recovery pulse sequence (t_1_ir_mb); T_2 relaxation times were measured using a Carr–Purcell–Meiboom–Gill pulse sequence (t_2_cp_mb). Magnetic resonance imaging was performed on an Agilent 4.7 T with a 120 mm actively shielded gradient coil. All samples were transferred into

dx.doi.org/10.1021/la500602x | *Langmuir* 2014, 30, 5873−5879

Eppendorf tubes and fixed on a homemade foam sample holder and then put into the coil. The parameter settings are TR = 50 ms, TE = 4.03 ms, matrix size = 128 × 128, and FOV = 70 mm × 35 mm.

2.4. *In Vitro* and *in Vivo* Fluorescent Imaging. A confocal laser scanning microscope (Olympus FV 500-IX81) was used to record cellular images. HeLa cells were plated in a 35 mm confocal dish (glass bottom dish) and grown to around 60% confluency for 24 h before the experiment. Cells were washed three times with DMEM, supplied with 1 mL DMEM, and then incubated with 100 μL of PMIDA-modified $Eu_{0.2}Gd_{0.8}PO_4{\cdot}H_2O$ nanoparticles. After 24 h of incubation, cells were washed three times with DMEM, supplied with 1 mL of DMEM, and then subjected to confocal fluorescence imaging. An argon laser (excitation wavelength of 488 nm) was used with a 60× oil-dispersion objective with a long pass filter at 560IF.

The same confocal laser scanning microscope was used to record *in vivo* fluorescent images of a small animal, *C. elegans*, with excitation at 488 nm and a 560IF filter. Food was prepared by mixing 200 μL of a solution of the nanoparticles that was 8 or 32 mM in Gd^{3+} with 200 μL of 100 mg/mL OP50 (a type of *E. coli*) in S-basal medium. Two hundred microliters of these solutions were pipetted out onto the assay plate and left to dry, which served as food for the worms. For the control group, no nanoparticles were added. The worms were starved for 48 h before they were fed for 4 h, followed by transferring into a 2 mL tube with water and holding at 65 °C for 5 min. Once prepared, the worms were imaged with a 10× objective.

2.5. Cytotoxicity Assay. The cytotoxicity of the $Eu_{0.2}Gd_{0.8}PO_4{\cdot}H_2O$ nanoparticles to HeLa and A549 cells was evaluated using the CellTiter 96 proliferation assay (Promega, Madison, WI, USA). A sample of 1×10^5 cells in 50 μL of fresh cell culture medium was seeded into each test well on a 96-well plate. After being cultured overnight, nanoparticles with different concentrations in 50 μL of fresh cell culture medium were added to the test wells. The resultant cell mixture was incubated at 37 °C under a 5% CO_2 atmosphere for 24 h. Then, 75 μL of the cell culture medium was removed from the test wells after centrifugation, and another 75 μL of fresh cell culture medium was added. The 96-well plate was then put back into the incubator for another 24 h. Finally, 20 μL of the CellTiter reagent was added to each test well, and the 96-well plate was subjected to absorption measurement at 490 nm using a VersaMax tunable microplate reader (Molecular Devices, Inc., Sunnyvale, CA).

3. RESULTS AND DISCUSSION

3.1. Particle Characterization. TEM images (Figure 1) of each preparation of $Eu_{0.2}Gd_{0.8}PO_4{\cdot}H_2O$ show uniform rodlike particles. The size distributions, shown in the histograms of Figure 1, give average particle sizes of 40 ± 4, 71 ± 14, and 145 ± 36 nm for samples **1**−**3**, respectively. The structure and composition of the particles were determined using powder XRD in conjunction with ICP-AES and EDS. The XRD patterns (Figure 2) from each sample can be indexed to the hexagonal phase of $GdPO_4{\cdot}H_2O$ (JCPDS no. 39-232) or $EuPO_4{\cdot}H_2O$ (JCPDS no. 20-1044), and no impurity phase was detected.[28] The resolution of the diffraction patterns does not discern between a homogeneous phase and a mixture of phases. However, EDS maps (Figure 2) clearly show the Eu and Gd ions are uniformly distributed within crystallites.

Particle surface modification provides colloidal stability and can be used to impart other functions such as biocompatibility or mechanisms for vectoring. The most common strategies include polymer modification and silica shell coating.[7,29] In the current study, we use the small-molecule PMIDA for postsynthesis surface modification following reports of its successful use for other metal phosphate and metal oxide particles.[30,31] The PMIDA molecule is expected to bind the particle surface through the divalent phosphate,[10,32] consistent with how it binds to $Ca_3(PO_4)_2$ and iron oxide surfaces.[30,31] After surface modification, the phosphate groups strongly bind with metal ions on the surface, leaving free carboxyl groups at the periphery, producing a well-dispersed suspension through electrostatic repulsions (Figure S1).

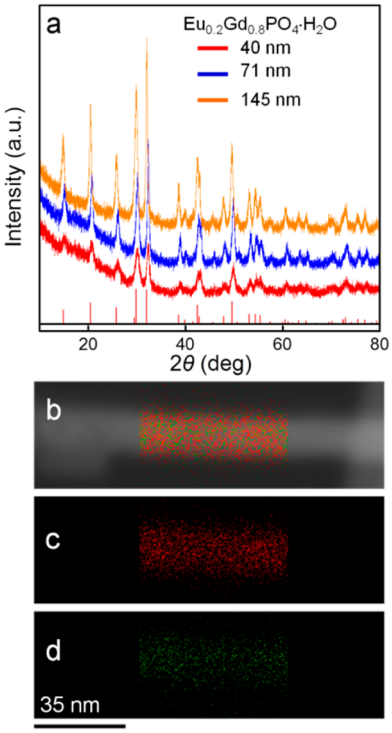

Figure 2. (a) XRD patterns of $Eu_{0.2}Gd_{0.8}PO_4{\cdot}H_2O$ samples **1**−**3** and a JCPDS file of hexagonal $GdPO_4{\cdot}H_2O$ (JCPDS no. 39-232) and EDS maps across a $Eu_{0.2}Gd_{0.8}PO_4{\cdot}H_2O$ nanoparticle; (b) overlapped Gd and Eu detection; (c) gadolinium map only; and (d) europium map only.

Our previous study of $GdPO_4{\cdot}H_2O$ particles modified with phosphate-terminated oligonucleotides showed that postsynthesis modification with excess Gd^{3+} to ensure a surface rich in Gd^{3+} led to increased binding of the oligonucleotide in addition to providing more water-accessible sites to influence the relaxivity.[10] This result was also observed here for PMIDA modification. FT-IR spectra confirm successful surface modification with PMIDA. Figure S2 compares FT-IR spectra of $Eu_{0.2}Gd_{0.8}PO_4{\cdot}H_2O$ before and after surface modification. The spectra are dominated by vibrations from the lattice PO_4^{3-} groups and water.[33] However, new bands at 2920 and 2851 cm^{-1} for the modified particles are associated with the asymmetric (ν_{as}) and symmetric (ν_s) stretching vibrations of methylene ($-CH_2$) groups of PMIDA.[31,34]

Surface modification with PMIDA provides an easy and direct procedure for obtaining dispersible and biocompatible particles. Furthermore, the terminal carboxyl groups of the PMIDA can be easily used for later functionalization with other biologically active molecules.[30,31,35]

3.2. Size-Dependent MRI Relaxivity. To begin to understand some of the factors that contribute to the range of relaxivity behavior reported for $GdPO_4{\cdot}H_2O$ and $Eu_xGd_{1-x}PO_4{\cdot}H_2O$ particles, samples of three different average particle sizes were prepared. Magnetic resonance relaxivity measurements of different concentrations of $Eu_{0.2}Gd_{0.8}PO_4{\cdot}H_2O$ particles dispersed in water were performed at 1.4 T to determine T_1 and T_2 values (Figure 3 and Table 1). The specific relaxivities were calculated according to

dx.doi.org/10.1021/la500602x | *Langmuir* 2014, 30, 5873−5879

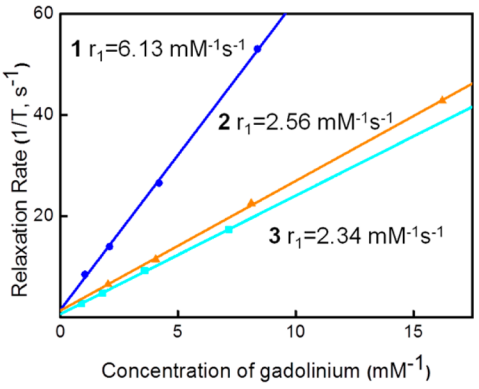

Figure 3. Plot of the proton relaxation rate $(1/T_1)$ of water suspensions of $Eu_{0.2}Gd_{0.8}PO_4{\cdot}H_2O$ nanoparticles at various Gd^{3+} concentrations and the corresponding relaxivites for samples **1** (40 nm), **2** (71 nm), and **3** (145 nm).

$$\frac{1}{T_{i_{app}}} = \frac{1}{T_i} + r_i \times [CA] \qquad i = 1,\ 2$$

where $T_{i_{app}}$ is the apparent T_1 or T_2, r_i represents relaxivities r_1 or r_2, and [CA] is the concentration of contrast agent.[36,37] The longitudinal relaxivity, r_1, ranges from 2.34 $mM^{-1}\ s^{-1}$ for the largest particles to 6.13 $mM^{-1}\ s^{-1}$ for the smallest.

The data in Figure 3 and Table 1 clearly show that the smaller particles give rise to higher molar relaxivity. Although the exact knowledge of how the gadolinium phosphate nanoparticles induce water proton relaxation is unknown, we would speculate that Gd^{3+} at the outer surface should contribute more to the relaxivity than ions in the core of the particle as water molecules have direct access to complexes at the surface.

The correlation between the S/V ratio and relaxivity of $Eu_{0.2}Gd_{0.8}PO_4{\cdot}H_2O$ nanoparticles is plotted in Figure 4. As expected, the smaller particle of sample **1** with the largest surface-to-volume ratio of 0.49 shows the highest relaxivity, which then decreases nearly linearly as the S/V ratio decreases, indicating that the availability of surface sites is primarily responsible for inducing relaxation.

The correlation with S/V ratio is in line with other studies of nanoparticle-based contrast agents. Relaxivity studies of Gd_2O_3 report that particles smaller than 10 nm have much higher r_1 than particles on the order of 30 nm diameter.[8,19,38] Similarly, r_1 values were found to be higher for smaller MnO particles, leading to speculation that the paramagnetic Mn^{2+} ions on the surface of the nanoparticles are responsible for the shortening of the T_1 relaxation times.[22] Both Rieter et al.[24] and Nishiyabu et al.[26] report on relaxivity studies with Gd^{3+}-MOF systems. In both cases, an inverse dependence on nanoparticle size was observed, with the smaller nanoparticles possessing a larger r_1 relaxivity, suggesting that the Gd^{3+} ions at or near the surface are primarily responsible for the observed relaxivities. Whether the availability of surface ions is the only important factor is unclear from these

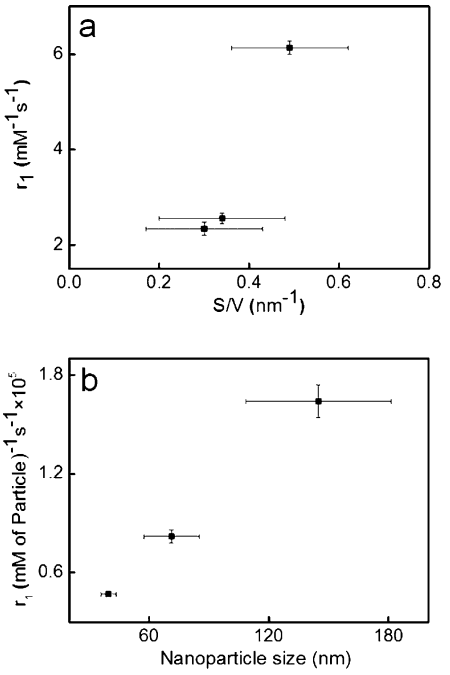

Figure 4. (a) Molar relaxivity, r_1, as a function of the surface-to-volume ratio, S/V, for samples **1**–**3**. (b) Relaxation enhancement per particle as a function of nanoparticle size.

observations, but certainly surface sites are the principal agents affecting the relaxivity with these paramagnetic metal oxide and metal phosphate systems.

Although the molar relaxivity decreases for larger particles, the relaxivity per particle can be significantly greater than for the small particles. Such a characteristic could allow for enhanced local contrast while using particle-based contrast agents, which would be highly beneficial for targeted imaging.[23] Recasting the relaxivity in units of relaxivity per particle,[24] $(mM\ particle)^{-1}\ s^{-1}$, shows the enhancement (Figure 4). The relaxivity per particle increases from 47 000 $(mM\ particle)^{-1}\ s^{-1}$ for the 40 nm particle to 164 000 $(mM\ particle)^{-1}\ s^{-1}$ for the 145 nm particles (Figure 4). Even for the larger particles, the per ion relaxivity is of the same order as for known gadolinium chelates,[13,20,39] but with so many more ions in a particle, they provide a mechanism to concentrate and localize the induced relaxation effectively.

With $r_1 = 6.13\ mM^{-1}\ s^{-1}$ and $r_2 = 7.78\ mM^{-1}\ s^{-1}$, the low value of $r_2/r_1 = 1.27$ suggests usefulness as a positive contrast agent. To demonstrate this, sample **1**, with the highest longitudinal relaxivity, was used to obtain T_1-weighted MR images. Figure 5 shows the T_1-weighted images obtained at 4.7 T at concentrations ranging up to 8 mM. Enhanced MRI brightness is observed with the increase in particle concentration.

It is useful to compare the relaxivity data for the materials described in this study to those of other gadolinium phosphate and Eu^{3+}-containing gadolinium phosphate systems.

Table 1. Size-Dependent Relaxivity Data for Samples 1–3

sample	length (nm)	width (nm)	molar relaxivity $r_1/[Gd^{3+}]$ $(mM^{-1}\ s^{-1})$	relaxation enhancement per nanoparticle r_1/NP $(mM\ particle)^{-1}\ s^{-1}$	surface-to-volume ratio $(nm^{-1})^a$
1	40 ± 4	9 ± 2	6.13 ± 0.14	47 000 ± 1000	0.49 ± 0.13
2	71 ± 14	13 ± 4	2.56 ± 0.11	82 000 ± 4000	0.34 ± 0.14
3	145 ± 36	14 ± 4	2.34 ± 0.14	164 000 ± 10 000	0.30 ± 0.13

[a]See Supporting Information

dx.doi.org/10.1021/la500602x | Langmuir 2014, 30, 5873–5879

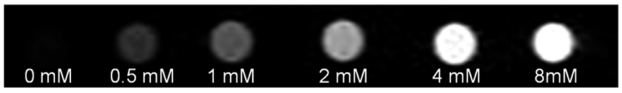

Figure 5. T_1-weighted MR images of $Eu_{0.2}Gd_{0.8}PO_4{\cdot}H_2O$ particles from sample **1** at various Gd^{3+} concentrations.

$Eu_{0.2}Gd_{0.8}PO_4{\cdot}H_2O$ samples **1**−**3** are compared to other reported particle systems in Table S1. Using particles containing 2% Eu^{3+}, Rodriguez-Liviano et al.[21] reported relaxivity values of $r_1 = 0.19\ mM^{-1}\ s^{-1}$ and $r_2 = 17.33\ mM^{-1}\ s^{-1}$ for $Eu_{0.02}Gd_{0.98}PO_4{\cdot}H_2O$, and by taking advantage of a large r_2/r_1 ratio, they used the particles to effectively generate negative contrast in MRI phantom images at 9.4 T. Interestingly, studies of $GdPO_4{\cdot}H_2O$ also report a wide range of relaxivities and r_2/r_1 ratios, with some studies emphasizing utility as positive contrast agents with others focusing on a large r_2 value and using the particles to demonstrate negative contrast. Particle size explains some of the differences, but it is clear that there are also other factors that influence the relaxivity behavior of the gadolinium phosphate system. In addition to the different particle sizes represented in Table S1, each study uses a different surface modifier. Details of the significance of these factors remain to be resolved.

3.3. Fluorescence Imaging. Suspensions of the particles exhibit strong visible fluorescence in the red region under UV irradiation, a result of the Eu^{3+} in the particles (Figure S3).[13,21] Such fluorescence properties have attracted considerable attention and show great potential for bioimaging applications. For example, Ren et al.[13] used Eu^{3+}-doped $GdPO_4$ nanorods modified with PVP to observe red luminescence from labeled HeLa cells. In addition, Patra et al.[18,40] successfully used pure $EuPO_4$ nanorods without a surface modifier to label both 786-O cells and HUVEC cells. To demonstrate the potential of the $Eu_{0.2}Gd_{0.8}PO_4{\cdot}H_2O$ system as a dual-imaging agent, the HeLa cells were imaged with confocal laser scanning microscopy following incubation with the PMIDA modified particles. After treatment, strong fluorescence was associated with nanoparticle uptake by the cells (Figure 6).

Further evidence of the fluorescence imaging potential of the particles is presented in Figure 7 showing confocal laser scanning microscopy images of *C. elegans* following inclusion of the $Eu_{0.2}Gd_{0.8}PO_4{\cdot}H_2O$ particles with different concentrations in the culture medium of the worms. Bright red fluorescence was observed due to the presence of the Eu^{3+} doped nanoparticles in *C. elegans*, where a stronger intensity can be seen when higher particle concentrations were used. No fluorescence was observed in the red region in the control. Together with the cell imaging and MRI contrast capability, these experiments demonstrate the potential of the PMIDA-modified $Eu_{0.2}Gd_{0.8}PO_4{\cdot}H_2O$ particle system for dual-imaging.

3.4. Cytotoxicity Measurements. When evaluating the clinical potential of nanoparticles, their toxicity is an important factor that should be taken into consideration. Therefore, we have studied the cytotoxicity of the as-prepared nanoparticles. Cytotoxicity testing was performed on PMIDA-modified $Eu_{0.2}Gd_{0.8}PO_4{\cdot}H_2O$ sample **1** using HeLa cells and A549 cells in solution up to 1 mM Gd^{3+}. As shown in Supporting Information (Figure S4), the average cell viability is 93 and 90% for HeLa cells and A549 cells, respectively. Therefore, PMIDA-coated $Eu_{0.2}Gd_{0.8}PO_4{\cdot}H_2O$ nanoparticles are nontoxic up to 1 mM Gd^{3+}.

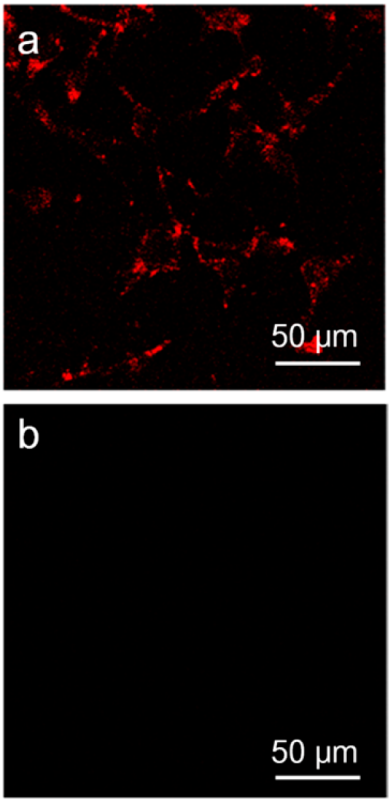

Figure 6. Confocal laser scanning microscopy images of Hela cells incubated (a) with and (b) without sample **1** nanoparticles.

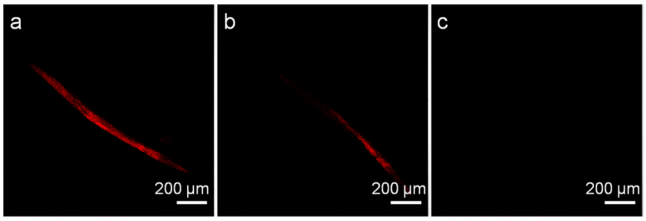

Figure 7. Confocal laser scanning microscopy images of *C. elegans* fed (a) with the higher concentration of nanoparticles (Materials and Methods), (b) with the lower concentration of nanoparticles, and (c) without nanoparticles.

4. CONCLUSIONS

The phosphate-containing PMIDA molecule stabilizes colloidal suspensions of particles of the mixed lanthanide $Eu_{0.2}Gd_{0.8}PO_4{\cdot}H_2O$, which with fluorescent Eu^{3+} ions and paramagnetic Gd^{3+} ions can be used for both fluorescence imaging and to generate MRI contrast. Relaxivity values vary with particle size, increasing with available surface area, implying that access to Gd^{3+} complexes at the surface is the principal factor influencing molar relaxivity. On the other hand, as the particles become larger, the relaxivity per particle increases, suggesting that larger particles might be useful for concentrating relaxivity effects in applications such as cellular or molecular imaging.

■ ASSOCIATED CONTENT

Supporting Information

Nanoparticle suspension images, FT-IR spectra, emission spectra, and cell viability test results. This material is available free of charge via the Internet at http://pubs.acs.org/.

dx.doi.org/10.1021/la500602x | *Langmuir* 2014, 30, 5873−5879

AUTHOR INFORMATION

Corresponding Author

*E-mail: talham@chem.ufl.edu.

Notes

The authors declare no competing financial interest.

ACKNOWLEDGMENTS

Funding is provided by the U.S. National Science Foundation Division of Chemistry under grant no. CHE-0957155, cofunded by the MPS/CHE and the Office of International Science and Engineering (DRT). The work is also supported by grants awarded by the National Institutes of Health, GM079359 and CA133086 (W.T.). We sincerely appreciate Xinxing Zhang and Dr. Rebecca Butcher for help with the *in vivo* experiment with *C. elegans*. We also thank Dr. Jan-Moritz Koenen and Dr. Kirk Schanze for help with acquiring fluorescence spectra. We are grateful to the McKnight Brain Institute at the University of Florida for the MRI technical support.

REFERENCES

(1) Gindy, M. E.; Prud'homme, R. K. Multifunctional Nanoparticles for Imaging, Delivery and Targeting in Cancer Therapy. *Drug Delivery* **2009**, *6*, 865−878.

(2) Liong, M.; Lu, J.; Kovochich, M.; Xia, T.; Ruehm, S. G.; Nel, A. E.; Tamanoi, F.; Zink, J. I. Multifunctional Inorganic Nanoparticles for Imaging, Targeting, and Drug Delivery. *ACS Nano* **2008**, *2*, 889−896.

(3) Chen, D.; Jiang, M.; Li, N.; Gu, H.; Xu, Q.; Ge, J.; Xia, X.; Lu, J. Modification of Magnetic Silica/Iron Oxide Nanocomposites with Fluorescent Polymethacrylic Acid for Cancer Targeting and Drug Delivery. *J. Mater. Chem.* **2010**, *20*, 6422−6429.

(4) Kim, D.; Jeong, Y. Y.; Jon, S. A Drug-Loaded Aptamer-Gold Nanoparticle Bioconjugate for Combined CT Imaging and Therapy of Prostate Cancer. *ACS Nano* **2010**, *4*, 3689−3696.

(5) Ow, H.; Larson, D. R.; Srivastava, M.; Baird, B. A.; Webb, W. W.; Wiesner, U. Bright and Stable Core-Shell Fluorescent Silica Nanoparticles. *Nano Lett.* **2005**, *5*, 113−117.

(6) Li, Y. L.; Zhu, L.; Liu, Z.; Cheng, R.; Meng, F.; Cui, J. H.; Ji, S. J.; Zhong, Z. Reversibly Stabilized Multifunctional Dextran Nanoparticles Efficiently Deliver Doxorubicin into The Nuclei of Cancer Cells. *Angew. Chem., Int. Ed.* **2009**, *48*, 9914−9918.

(7) Chen, F. H.; Zhang, L. M.; Chen, Q. T.; Zhang, Y.; Zhang, Z. J. Synthesis of a Novel Magnetic Drug Delivery System Composed of Doxorubicin-Conjugated Fe_3O_4 Nanoparticle Cores and a PEG-Functionalized Porous Silica Shell. *Chem. Commun.* **2010**, *46*, 8633−8635.

(8) Bridot, J. L.; Faure, A. C.; Laurent, S.; Riviere, C.; Billotey, C.; Hiba, B.; Janier, M.; Josserand, V.; Coll, J. L.; Elst, L. V.; Muller, R.; Roux, S.; Perriat, P.; Tillement, O. Hybrid Gadolinium Oxide Nanoparticles: Multimodal Contrast Agents for *In Vivo* Imaging. *J. Am. Chem. Soc.* **2007**, *129*, 5076−5084.

(9) Ryu, J.; Park, H.-Y.; Kim, K.; Kim, H.; Yoo, J. H.; Kang, M.; Im, K.; Grailhe, R.; Song, R. Facile Synthesis of Ultrasmall and Hexagonal $NaGdF_4$: Yb^{3+}, Er^{3+} Nanoparticles with Magnetic and Upconversion Imaging Properties. *J. Phys. Chem. C* **2010**, *114*, 21077−21082.

(10) Dumont, M. F.; Baligand, C.; Li, Y.; Knowles, E. S.; Meisel, M. W.; Walter, G. A.; Talham, D. R. DNA Surface Modified Gadolinium Phosphate Nanoparticles as MRI Contrast Agents. *Bioconjugate Chem.* **2012**, *23*, 951−957.

(11) Talanov, V. S.; Regino, C. A.; Kobayashi, H.; Bernardo, M.; Choyke, P. L.; Brechbiel, M. W. Dendrimer-Based Nanoprobe for Dual Modality Magnetic Resonance and Fluorescence Imaging. *Nano Lett.* **2006**, *6*, 1459−1463.

(12) Insin, N.; Tracy, J. B.; Lee, H.; Zimmer, J. P.; Westervelt, R. M.; Bawendi, M. G. Incorporation of Iron Oxide Nanoparticles and Quantum Dots into Silica Microspheres. *ACS Nano* **2008**, *2*, 197−202.

(13) Ren, W.; Tian, G.; Zhou, L.; Yin, W.; Yan, L.; Jin, S.; Zu, Y.; Li, S.; Gu, Z.; Zhao, Y. Lanthanide Ion-Doped $GdPO_4$ Nanorods with Dual-Modal Bio-Optical and Magnetic Resonance Imaging Properties. *Nanoscale* **2012**, *4*, 3754−3760.

(14) Rodriguez-Liviano, S.; Nuñez, N. O.; Rivera-Fernández, S.; de la Fuente, J. M.; Ocaña, M. Ionic Liquid Mediated Synthesis and Surface Modification of Multifunctional Mesoporous Eu:GdF_3 Nanoparticles for Biomedical Applications. *Langmuir* **2013**, *29*, 3411−3418.

(15) Jung, J.; Kim, M. A.; Cho, J. H.; Lee, S. J.; Yang, I.; Cho, J.; Kim, S. K.; Lee, C.; Park, J. K. Europium-Doped Gadolinium Sulfide Nanoparticles as a Dual-Mode Imaging Agent for T_1-Weighted MR and Photoluminescence Imaging. *Biomaterials* **2012**, *33*, 5865−5874.

(16) Shi, Z.; Neoh, K. G.; Kang, E. T.; Shuter, B.; Wang, S. C. Bifunctional Eu^{3+}-Doped Gd_2O_3 Nanoparticles as a Luminescent and T_1 Contrast Agent for Stem Cell Labeling. *Contrast Media Mol. Imaging* **2010**, *5*, 105−111.

(17) Petoral, R. M.; Söderlind, F.; Klasson, A.; Suska, A.; Fortin, M. A.; Abrikossova, N.; Selegård, L.; Käll, P.-O.; Engström, M.; Uvdal, K. Synthesis and Characterization of Tb^{3+}-Doped Gd_2O_3 Nanocrystals: A Bifunctional Material with Combined Labeling and MRI Contrast Agent Properties. *J. Phys. Chem. C* **2009**, *113*, 6913−6920.

(18) Patra, C. R.; Bhattacharya, R.; Patra, S.; Basu, S.; Mukherjee, P.; Mukhopadhyay, D. Inorganic Phosphate Nanorods Are a Novel Fluorescent Label in Cell Biology. *J. Nanobiotechnol.* **2006**, *4*, 1−15.

(19) Park, J. Y.; Baek, M. J.; Choi, E. S.; Woo, S.; Kim, J. H.; Kim, T. J.; Jung, J. C.; Chae, K. S.; Chang, Y.; Lee, G. H. Paramagnetic Ultrasmall Gadolinium Oxide Nanoparticles as Advanced T_1 MRI Contrast Agent: Account for Large Longitudinal Relaxivity, Optimal Particle Diameter, and *In Vivo* T_1 MR Images. *ACS Nano* **2009**, *3*, 3663−3669.

(20) Hifumi, H.; Yamaoka, S.; Tanimoto, A.; Citterio, D.; Suzuki, K. Gadolinium-Based Hybrid Nanoparticles as a Positive MR Contrast Agent. *J. Am. Chem. Soc.* **2006**, *128*, 15090−15091.

(21) Rodriguez-Liviano, S.; Becerro, A. I.; Alcántara, D.; Grazú, V.; de la Fuente, J. M.; Ocaña, M. Synthesis and Properties of Multifunctional Tetragonal Eu:$GdPO_4$ Nanocubes for Optical and Magnetic Resonance Imaging Applications. *Inorg. Chem.* **2013**, *52*, 647−654.

(22) Na, H. B.; Lee, J. H.; An, K.; Park, Y. I.; Park, M.; Lee, I. S.; Nam, D. H.; Kim, S. T.; Kim, S. H.; Kim, S. W.; Lim, K. H.; Kim, K. S.; Kim, S. O.; Hyeon, T. Development of a T_1 Contrast Agent for Magnetic Resonance Imaging Using MnO Nanoparticles. *Angew. Chem., Int. Ed.* **2007**, *119*, 5493−5497.

(23) Johnson, N. J. J.; Oakden, W.; Stanisz, G. J.; Scott Prosser, R.; van Veggel, F. C. J. M. Size-Tunable, Ultrasmall $NaGdF_4$ Nanoparticles: Insights into Their T_1 MRI Contrast Enhancement. *Chem. Mater.* **2011**, *23*, 3714−3722.

(24) Rieter, W. J.; Taylor, K. M. L.; An, H.; Lin, W.; Lin, W. Nanoscale Metal-Organic Frameworks as Potential Multimodal Contrast Enhancing Agents. *J. Am. Chem. Soc.* **2006**, *128*, 9024−9025.

(25) Della Rocca, J.; Liu, D.; Lin, W. Nanoscale Metal-Organic Frameworks for Biomedical Imaging and Drug Delivery. *Acc. Chem. Res.* **2011**, *44*, 957−968.

(26) Nishiyabu, R.; Hashimoto, N.; Cho, T.; Watanabe, K.; Yasunaga, T.; Endo, A.; Kaneko, K.; Niidome, T.; Murata, M.; Adachi, C.; Katayama, Y.; Hashizume, M.; Kimizuka, N. Nanoparticles of Adaptive Supramolecular Networks Self-Assembled from Nucleotides and Lanthanide Ions. *J. Am. Chem. Soc.* **2009**, *131*, 2151−2158.

(27) Lu, S.; Zhang, J.; Zhao, H.; Luo, Y.; Ren, X. Remarkably Enhanced Photoluminescence of Hexagonal $GdPO_4{\cdot}nH_2O$:Eu with Decreasing Size. *Nanotechnology* **2010**, *21*, 365709.

(28) Sahu, N. K.; Ningthoujam, R. S.; Bahadur, D. Disappearance and Recovery of Luminescence in $GdPO_4$:Eu^{3+} Nanorods: Propose to Water/$OH^{\bullet}$ Release under Near Infrared and Gamma Irradiations. *J. Appl. Phys.* **2012**, *112*, 014306.

(29) Gupta, A. K.; Gupta, M. Synthesis and Surface Engineering of Iron Oxide Nanoparticles for Biomedical Applications. *Biomaterials* **2005**, *26*, 3995−4021.

(30) Rout, S. R.; Behera, B.; Maiti, T. K.; Mohapatra, S. Multifunctional Magnetic Calcium Phosphate Nanoparticles for Targeted Platin Delivery. *Dalton Trans.* **2012**, *41*, 10777−10783.

(31) Das, M.; Mishra, D.; Dhak, P.; Gupta, S.; Maiti, T. K.; Basak, A.; Pramanik, P. Biofunctionalized, Phosphonate-Grafted, Ultrasmall Iron Oxide Nanoparticles for Combined Targeted Cancer Therapy and Multimodal Imaging. *Small* **2009**, *5*, 2883−2893.
(32) Queffélec, C.; Petit, M.; Janvier, P.; Knight, D. A.; Bujoli, B. Surface Modification Using Phosphonic Acids and Esters. *Chem. Rev.* **2012**, *112*, 3777−3807.
(33) Huang, C. C.; Lo, Y. W.; Kuo, W. S.; Hwu, J. R.; Su, W. C.; Shieh, D. B.; Yeh, C. S. Facile Preparation of Self-Assembled Hydrogel-Like $GdPO_4{\cdot}H_2O$ Nanorods. *Langmuir* **2008**, *24*, 8309−8913.
(34) Bhattacharya, D.; Baksi, A.; Banerjee, I.; Ananthakrishnan, R.; Maiti, T. K.; Pramanik, P. Development of Phosphonate Modified $Fe_{(1-x)}Mn_xFe_2O_4$ Mixed Ferrite Nanoparticles: Novel Peroxidase Mimetics in Enzyme Linked Immunosorbent Assay. *Talanta* **2011**, *86*, 337−348.
(35) Medley, C. D.; Bamrungsap, S.; Tan, W.; Smith, J. E. Aptamer-Conjugated Nanoparticles for Cancer Cell Detection. *Anal. Chem.* **2011**, *83*, 727−734.
(36) Gillis, P.; Koening, S. H. Transverse Relaxation of Solvent Protons Induced by Magnetized Spheres: Application to Ferritin, Erythrocytes, and Magnetite. *Magn. Reson. Med.* **1987**, *5*, 323−345.
(37) Arsalani, N.; Fattahi, H.; Nazarpoor, M. Synthesis and Characterization of PVP-Functionalized Superparamagnetic Fe_3O_4 Nanoparticles as an MRI Contrast Agent. *Polym. Lett.* **2010**, *4*, 329−338.
(38) Fortin, M. A.; Petoral, R. M.; Söderlind, F.; Klasson, A.; Engström, M.; Veres, T.; Käll, P. O.; Uvdal, K. Polyethylene Glycol-Covered Ultra-Small Gd_2O_3 Nanoparticles for Positive Contrast at 1.5 T Magnetic Resonance Clinical Scanning. *Nanotechnology* **2007**, *18*, 395501.
(39) Bottrill, M.; Kwok, L.; Long, N. J. Lanthanides in Magnetic Resonance Imaging. *Chem. Soc. Rev.* **2006**, *35*, 557−571.
(40) Patra, C. R.; Bhattacharya, R.; Patra, S.; Basu, S.; Mukherjee, P.; Mukhopadhyay, D. Lanthanide Phosphate Nanorods as Inorganic Fluorescent Labels in Cell Biology Research. *Clin. Chem.* **2007**, *53*, 2029−2031.